Supporting Information

Programmable Light-Controlled Shape Changes in Layered Polymer Nanocomposites

Zhichen Zhu, Erkan Senses, Pinar Akcora and Svetlana Sukhishvili*

Stevens Institute of Technology, Hoboken, NJ 07030

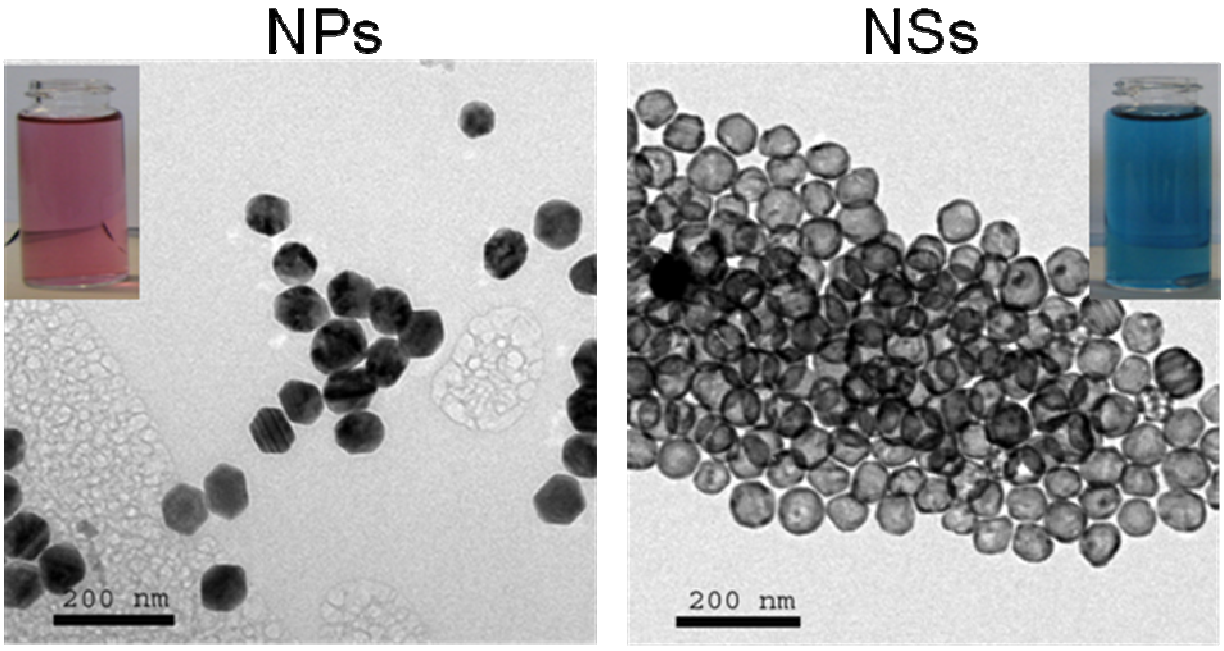

Figure S1. TEM images of synthesized gold NPs with diameter 70±10 nm (left) and gold NSs with diameter 65±6 nm.

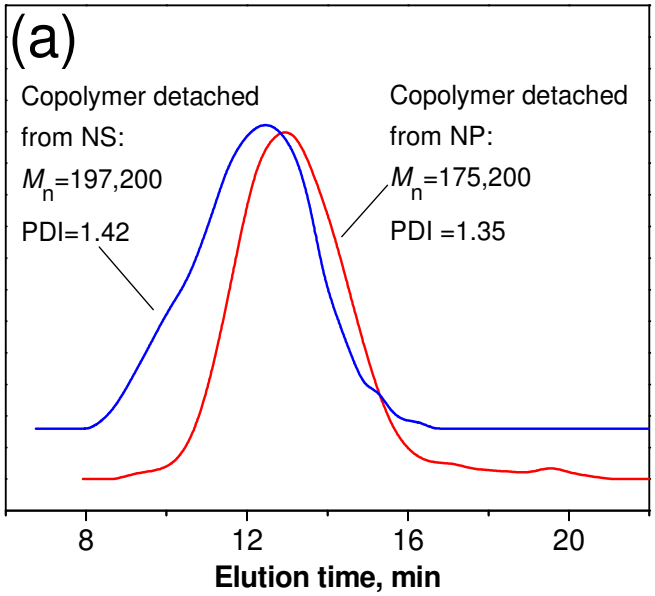

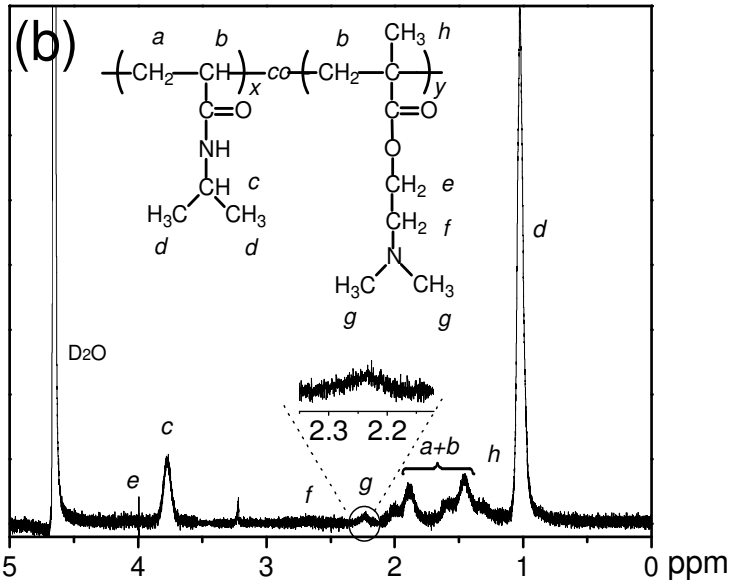

Figure S2. (a) GPC profiles of DMF solutions of poly(NIPAM-*co*-DMA) chains detached from gold NPs and NSs, respectively; (b) ^{1}H NMR spectrum of D_2O solution of poly(NIPAM-*co*-DMA) chains detached from gold NPs.

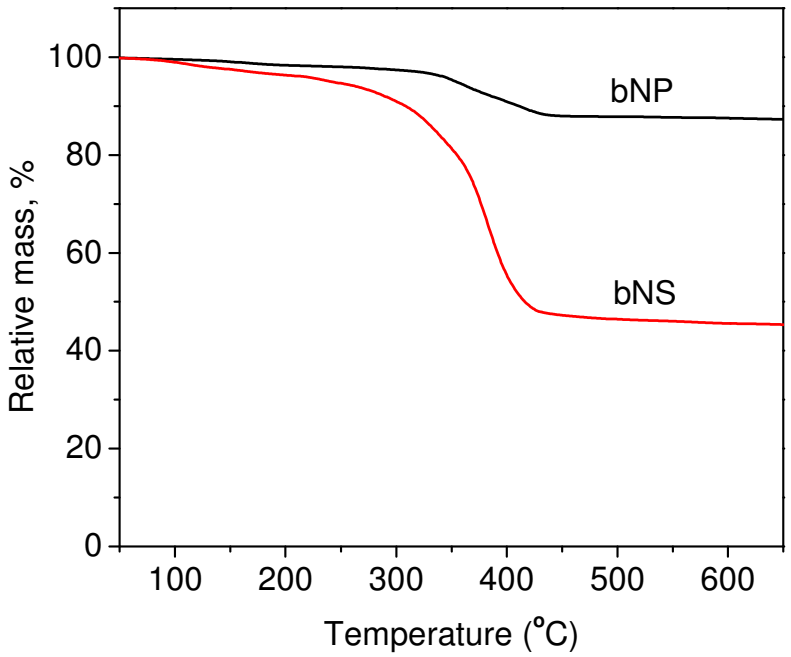

Figure S3. TGA of bNPs and bNSs, performed at a heating rate of 20°C/min under nitrogen atmosphere. The analysis revealed the 86.7 wt% and 44.8 wt% gold content for bNP and bNS, respectively.

An example of calculation of copolymer grafting density for bNPs

From the 86.7 % weight content of gold in bNP, the average diameter of a nanoparticle core of 70 nm determined by TEM (Figure S1), and the bulk gold density of 19.32 g/cm³, masses of a single nanoparticle and that of an individual polymer shell (3.47×10^{-16} g and 5.32×10^{-15}g, respectively) have been calculated. By dividing the latter value by the weight of a single polymer chain (calculated from the GPC-determined molecular weight of 175,000 g/mol), the average number of chains per particle was calculated to be 1830. Finally, through the additional calculation of the nanoparticle surface area, the graft density of 0.12 chains per nm² was obtained.

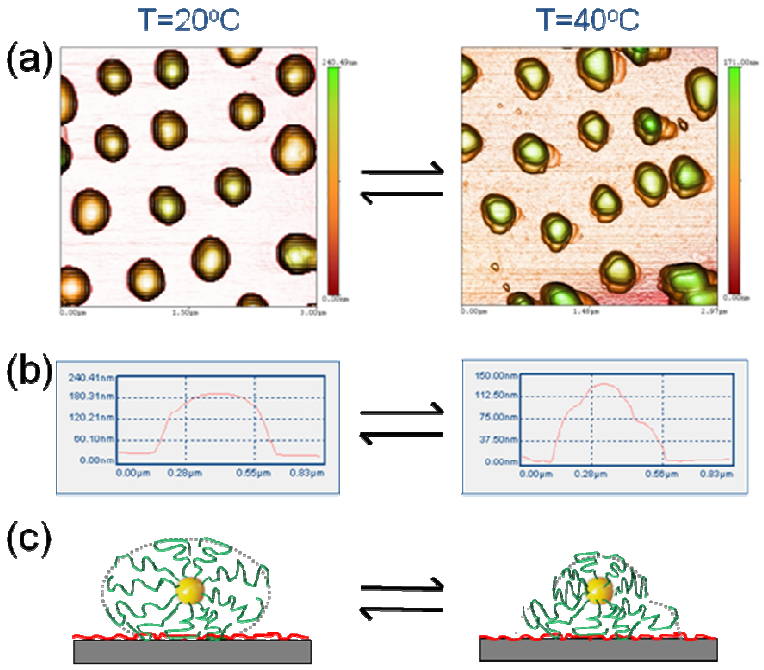

Figure S4. (a) *In-situ* AFM demonstration of temperature-induced morphological changes with bNPs adsorbed at the surface of a silicon wafer in 0.01M phosphate buffer at pH 3.0. The surface of silicon wafer was coated with a single layer of PMAA (adsorbed from 0.2 mg/ml solutions at pH 3) in order to provide the substrate with centers of hydrogen bonding with NIPAM units of bNPs. (b), (c) AFM height profiles and a schematic drawing of surface-adsorbed bNPs, respectively, showing a temperature-induced, reversible sphere-to-hat transition.

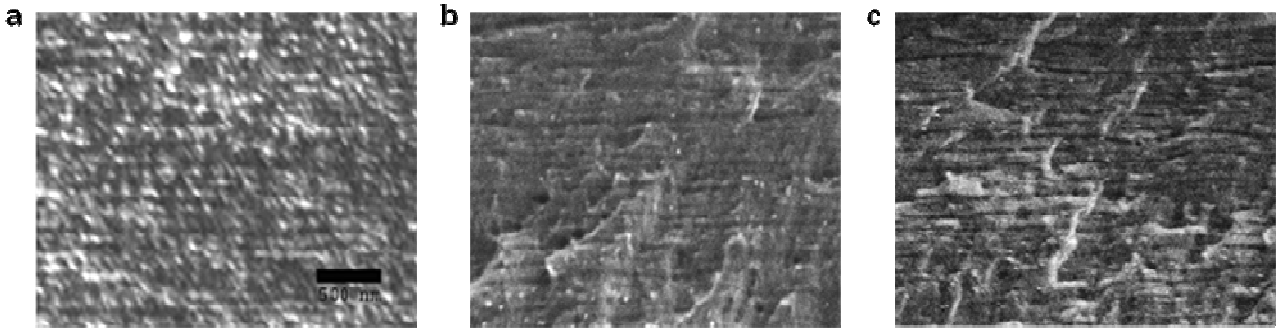

Figure S5. **Internal structure of bNP-containing films.** SEM images showing cross-sections of spin-deposited bNP_1-pol_{10} (a), bNP_1-pol_{30} (b), and bNP_1-pol_{50} (c) multilayers. All multilayer films were cut in the dry state with a razor blade.

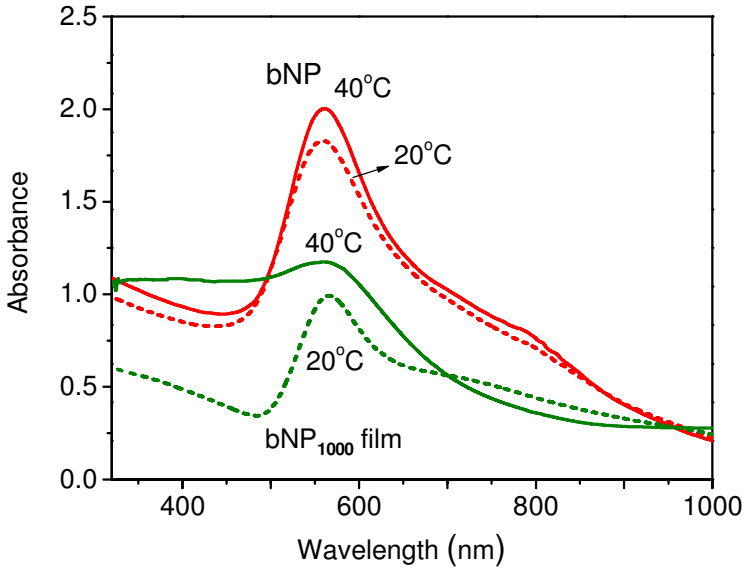

Figure S6. UV-Vis spectra of a 1% (by weight) solution of bNPs dispersed in 0.01 M phosphate buffer at pH 3 (top curves), and a bNP_{1000} film immersed in 0.01M phosphate buffer at pH 3 (bottom curves), measured at 20 ^{o}C or 40 ^{o}C.

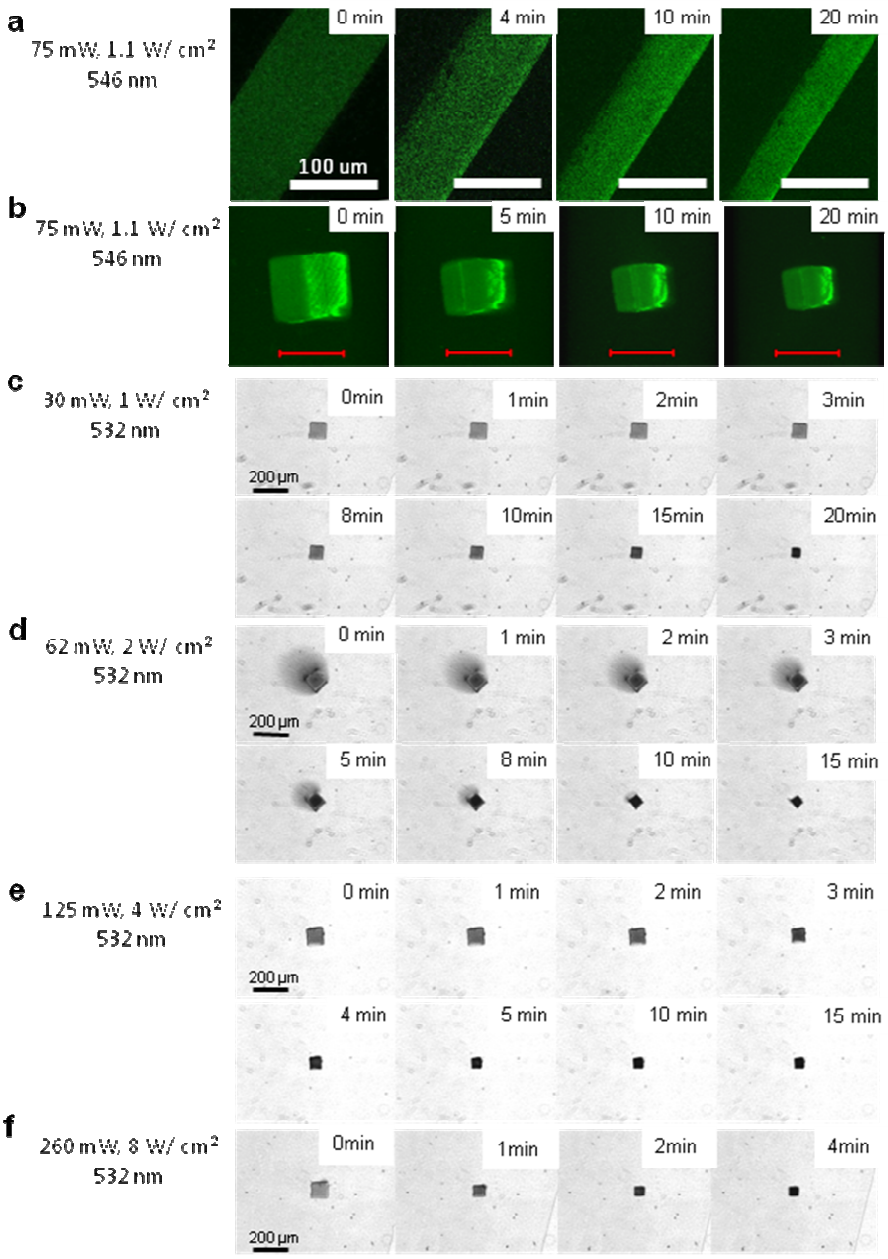

Figure S7. Deswelling kinetics of bNP assemblies. CLSM images of bNP_{500} film deposited on the surface of a glass slide (**a**), and a cube microtomed from a bNP_{500} film swollen at 25°C, upon exposure to 546-nm band-pass-filtered mercury lamp irradiation at 1.1 W/cm^2 (**b**). **c-f,** Optical microscopy images illustrating deswelling kinetics of cubes microtomed from bNP_{500} films swollen at 25°C upon exposure to 532-nm laser irradiation at power densities 1 to 8 W/cm^2.

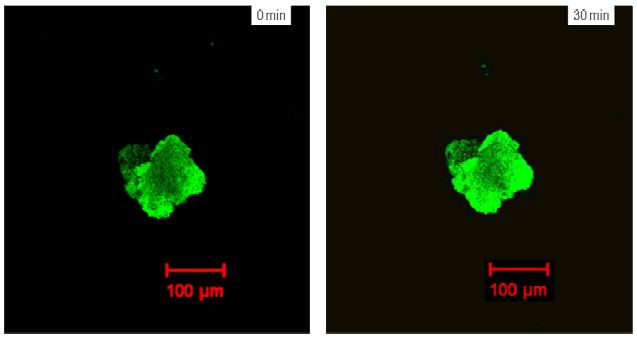

Figure S8. Control experiment: PNIPAM gel under irradiation. CLSM images of a cube microtomed from 2% cross-linked PNIPAM gel (water, 25°C) as a function of exposure time to 546-nm-filtered mercury lamp irradiation of 1.1 W/cm^2.

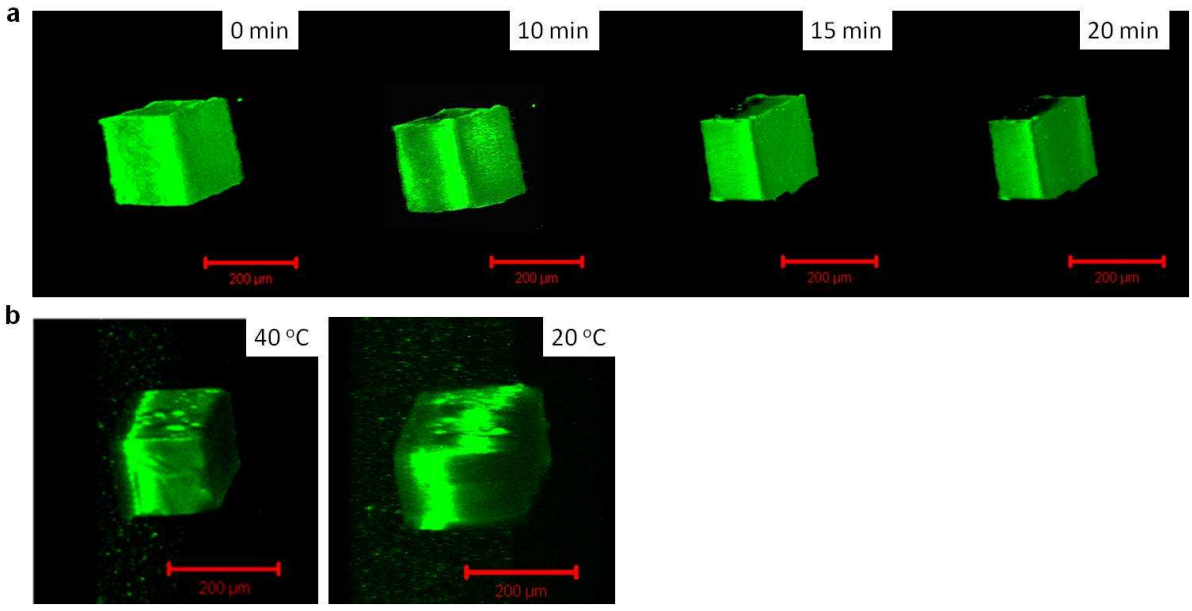

Figure S9. **Anisotropic shape changes in cubes cut from bNP-pol$_{30}$ hybrid films. a,** CLSM images showing anisotropic deswelling of bNP$_1$-pol$_{30}$ cubes (cut from a wet film swollen at 25°C) upon exposure to 1.1-W/cm^2 546-nm-filtered mercury lamp irradiation. **b,** CLSM images showing anisotropic swelling of a bNP$_1$-pol$_{30}$ cube (cut from a dry film) in solutions at 40 and 20 ºC.

Temperature Sweep Experiments. Swollen samples with thicknesses of ~0.8 mm were cut into disc shapes of ~12-mm diameter and inserted within the gap between the plates. Initial diameters of the samples were chosen to be larger than the diameters of the parallel plates in order to compensate for sample shrinkage in the radial direction. The additional material remaining out of the gap does not affect the results (Figure S9). For the bulk swollen sample of 0.8 mm thickness, the k_h value is estimated be 0.0625 s^{-1} (or we can say on the order of 0.1 s^{-1} since it is just a scaling) by using half of the sample thickness as the characteristic length for heat diffusion.

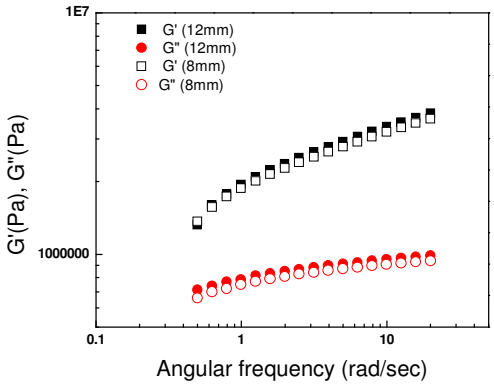

Figure S10. Control experiment indicating that the sample diameter had no effect on the measured values of moduli. The frequency sweep data obtained at a 0.2% strain amplitude for swollen $[bNP_1\text{-}pol_{30}]_{500}$ hybrid films at 25°C.

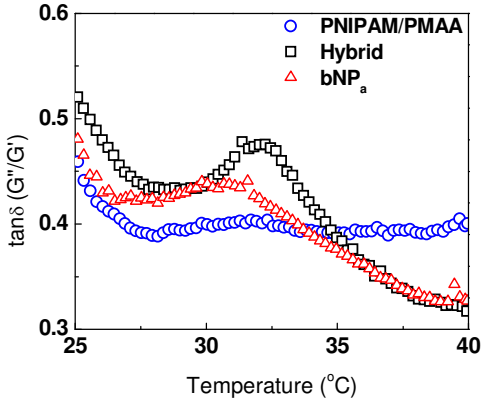

Figure S11. **Temperature effects on loss tangent of polymer-bNP assemblies.** Loss tangent curves constructed using rheology measurements for bNP_{1000}, pol_{5000} and $[bNP_1\text{-}pol_{30}]_{500}$ hybrid films.

Heat Transfer Model Around a Heating Source. We modeled heat transfer in the collapsing brush with the assumption that heat transfer takes place as conduction within collapsed polymer layer and as convection in the swollen part during the LCST transition. We take the thermal conductivity of the collapsed layer (k_b) as 0.05 W/m^2-K, the convective heat transfer coefficient (h) as 20 W/m^2-K and the thermal conductivity of gold nanoparticle (k_p) as 300 W/m^2-K. We solved the temperature distribution around a nanoparticle with a moving boundary condition at the brush surface controlled by the heat convection. The notation q_r means heat flux in the r-direction. T_b, T_w and T_p are the temperatures at the surface of collapsed polymer layer, water and particles, respectively. R_p is the particle radius, and R_b is the radius of particle with the collapsing brush layer. Solving the following equations with the boundary conditions,

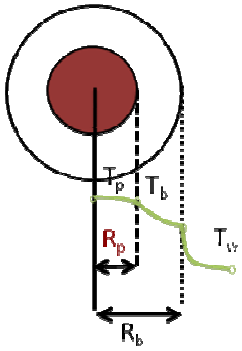

$$-\frac{1}{r^2}\frac{\partial}{\partial r}(r^2 q_r{}^p) + S_0 = 0 \qquad \text{For } 0<r<R_p$$

$$-\frac{1}{r^2}\frac{\partial}{\partial r}(r^2 q_r{}^b) = 0 \qquad \text{For } R_p<r<R_b$$

B.C.1: At r=0, T_p is finite
B.C.2: At r=R_p, T is continuous
B.C.3: At r=R_p, $-k_p (dT_p/dr)=-k_b (dT_b/dr)$
B.C.4: At r=R_b, $-k_b (dT_b/dr)=h(T_b-T_w)$

temperature distribution in the collapsed brush layer is obtained as:

$$T_b - T_w = \Delta T = \frac{1}{2}\frac{S_0 . R_p^2 (\ln(\frac{R_b}{r}) + \frac{k_b}{R_b h})}{k_b}$$

The solution to this temperature profile at varying source powers is shown in Fig. S10. As is seen in the Figure, brush collapse occurs at power densities above ~ 0.7 W/cm^2 and at 32^{o}C (LCST) the thickness of the collapsed layer reaches its maximum value of 90 nm (as shown by the dashed line). This model is for a single brush shrinking isotropically at steady-state. We conjecture that non-uniform temperature distribution may occur in anisotropic swelling, therefore heat transfer can contribute to anisotropic shrinkage along with mechanical stresses restricted by PNIPAM/PMAA layers in the xy-direction.

Thermal diffusion is related to the heat transfer rate as $k_h \approx \frac{\alpha}{L^2}$, where k_h is the heat transfer rate; L is the characteristic length for heat diffusion and α is the thermal diffusivity. Using a typical thermal diffusivity of ~10^{-8} m^2/sec and L of 80 ·10^{-9} m (radius of the collapsed layer), k_h *i*s found to be on the order of 10^7 s^{-1}.

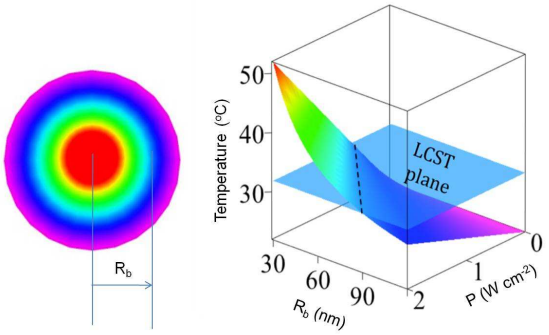

Figure S12. Temperature profile around a nanoparticle as a function of power density and collapsed brush layer thickness (R_b), calculated using heat conduction model around a spherical heating source.

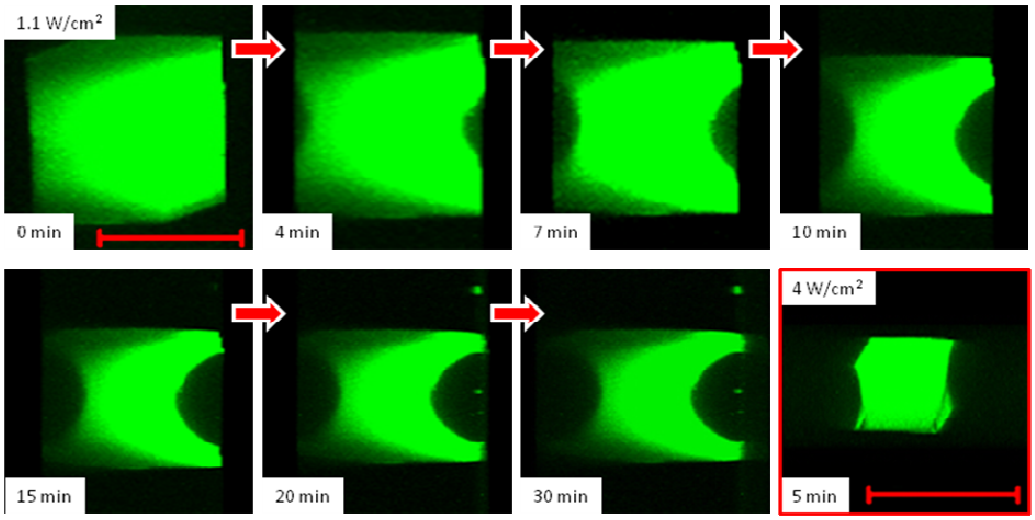

Figure S13. **Light-triggered spatially-resolved shape changes in triple-stratum bNS-bNP-bNS assemblies.** CLSM 3D images of bNS_{300}-bNP_{400}-bNS_{300} cubes cut from films pre-swollen at 25°C, under irradiation with a 546-nm-filtered mercury lamp with the power density 1.1 W/cm^2 (top row) and with a 532-nm laser at 4 W/cm^2 (bottom row). The scale bar is 200 μm.